Contents lists available at ScienceDirect

Arabian Journal of Chemistry

journal homepage: www.ksu.edu.sa

Original article

Antidiabetic activity of *Siraitia grosvenorii*, *Dimocarpus longan* Lour. and *Orthosiphon stamineus* Benth. Extracts combinations *in vitro* and *in silico*

Jing Zhao [a], Douglas Law [b], Song Zhu [a,e], Thiam-Tsui Tee [c], Cheah Yew Hoong [c], Ahmed Najm [a,*], Shazrul Fazry [a,d,*]

[a] *Department of Food Sciences, Faculty of Science and Technology, Universiti Kebangsaan Malaysia, 43600 Bangi, Selangor, Malaysia*
[b] *Faculty of Health and Life Sciences, Inti International University, 71800 Nilai, Negeri Sembilan, Malaysia*
[c] *ZACH Biotech Depot Sdn. Bhd., No. 19-2, Jalan SC 5/A, Kawasan Perindustrian Sg. Chua, 43000 Kajang, Selangor, Malaysia*
[d] *Tasik Chini Research Center, The Centre for Natural and Physical Laboratory Management, Universiti Kebangsaan Malaysia, 43600 Bangi, Selangor, Malaysia*
[e] *Heze medical college, Heze, Shandong 274000, China*

ARTICLE INFO

Keywords:
Antidiabetic
Glucose uptake
Molecular docking
Molecular dynamics simulation

ABSTRACT

Due to the economic burden created by diabetes, it is imperative to explore the potential of common dietary sources as complementary remedies for diabetic sufferers. The present study aims to evaluate the synergistic antidiabetic activity of combined extracts from *Siraitia grosvenorii, Dimocarpus longan, and Orthosiphon stamineus in silico* and *in vitro*, which include DPPH radical scavenging capacity, α-amylase inhibition, α-glucosidase inhibition, DPP-4 inhibition, cytotoxicity, and glucose uptake kinetics. The combination of *S. grosvenorii* + *Dimocarpus longan* + *O. stamineus (SG + DL + OS)* showed potential in inhibiting DPPH with an IC_{50} value of 7.21 ± 0.72 mg/ml, which also exhibited inhibitory effects on α-amylase, α-glucosidase, and DPP-4, with IC_{50} values of 8.63 ± 0.35 mg/ml, 5.41 ± 0.67 mg/ml, and 2.89 ± 0.09 mg/ml, respectively. Furthermore, it has been observed that the glucose uptake of L6 myoblasts can be significantly enhanced ($P < 0.05$) by treating different combinations. According to the results of XP docking and MM-GBSA analysis *in silico*, 26 and 32 compounds in the combination have significant interaction and stable binding ability with α-amylase and DPP-4 proteins, which can be used as α-amylase and DPP-4 inhibitors. Hence, it can be concluded that combinations of *S. grosvenorii*, *D. longan*, and *O. stamineus* have presented a viable therapeutic option for managing diabetes.

1. Introduction

Diabetes mellitus (DM) is a prevalent metabolic disorder characterized by abnormal insulin production or insulin resistance, leading to a significant elevation in glucose levels (Tomic et al., 2022). It often presents with symptoms including increased thirst, frequent urination, blurred vision, and weight loss (Entezari et al., 2022). Recently, the worldwide prevalence of diabetes has surged, imposing a significant economic burden on many nations and societies (Liu et al., 2023). Currently, oral hypoglycemic drugs and insulin constitute the primary treatments for diabetes. However, these medications frequently exhibit adverse effects and drug tolerance, driving individuals to explore more effective and fewer side-effect alternatives (Liu et al., 2022). Natural plant extracts are a substantial source of auxiliary and therapeutic bioactive chemicals, which are extensively utilized in the research and development of active pharmaceuticals (Rahman et al., 2022). These are considered more readily available, cost-effective, and more efficacious than synthetic drugs (Ansari et al., 2022). In fact, plant extracts have been employed to manage diabetes in numerous countries for a long time (Yusuf et al., 2022).

Previous research has found that *Siraitia grosvenorii* (*luo han guo*), *Dimocarpus longan* Lour. (*longan*) and Orthosiphon stamineus Benth (*Misai Kucing*) both have antidiabetic properties (Bassalat et al., 2023, Gong et al., 2022, Tang *et al.*, 2019), and our detection also verified this. Mogrosides and polysaccharides extracted from *S. grosvenorii* can effectively regulate and improve insulin resistance and control blood sugar levels to accomplish anti-diabetes effects (Liu et al., 2019, Zhang et al., 2021). The extracts from *longan* peel and seeds shows anti-diabetic and anti-hyperglycemic effects in both *in vivo* and *in vitro* study models by enhancing gene expression associated with insulin production and

* Corresponding author at: Department of Food Sciences, Faculty of Science and Technology, Universiti Kebangsaan Malaysia, 43600 Bangi, Selangor, Malaysia.
E-mail addresses: p114682@siswa.ukm.edu.my (J. Zhao), thiamtsu@zachbiotech.com (T.-T. Tee), yhcheah@zachbiotech.com (C. Yew Hoong), ahmadaljemeely@gmail.com (A. Najm), shazrul@ukm.edu.my (S. Fazry).

https://doi.org/10.1016/j.arabjc.2024.105733
Received 15 November 2023; Accepted 13 March 2024
Available online 14 March 2024

inhibiting glucosidase activity (Rakariyatham et al., 2020). *Orthosiphon stamineus* Benth (*Misai Kucing*) is a traditional medicinal plant abundantly spread in tropical and subtropical regions, and widely used as dietary supplements and for herbal and ornamental purposes (Wang et al., 2022). According to the most recent study, *O. stamineus* can combat diabetes by scavenging the oxidants, enhancing GLUT4 translocation, and inhibiting PTP1B activity (Bassalat et al., 2023, Nguyen, 2019).

Ayurveda and traditional Chinese medicine advocate multi-herbal formula therapy, positing that blending or combining two or more types of herbs can yield better therapeutic outcomes compared to individual herbs (Perumal et al., 2022). Considering that the activity of the single extracts of these three plants and the combination of multi-extracts may have better and longer-lasting therapeutic potential than single plant extracts, this study aims to investigate the combination of anti-diabetic activity of *S. grosvenorii*, *D. longan*. and *O. stamineus* extracts.

2. Materials and methods

2.1. Chemicals and reagents

Sodium carbonate (NaCO3), gallic acid, quercetin, 2,2-Diphenyl-1-picrylhydrazyl (DPPH), sodium nitrite ($NaNO_2$), sodium hydroxide (NaOH), sodium chloride ($NaCl_2$), α-glycosidase, α-amylase, p-nitrophenyl-α-D-glucopyranoside (PNPG), iodin and trolox were purchased from Sigma-Aldrich. Aluminum chloride solution (AlCl3), Folin-Ciocalteu reagent, and starch were procured from Merck. Dulbecco's modified Eagle medium (DMEM) and fetal bovine serum (FBS) were purchased from Fisher Scientific. All chemicals and reagents were analytical grades. Ethanol, methanol, and hydrochloric acid (HCl) were of analytical grade purchased from Fisher Scientific.

2.2. Preparation of extraction

2.2.1. Crude extract of S. grosvenorii fruit

Ripe *S. grosvenorii* fruit (Guilin, China) with the epidermis removed was completely dried at 40 °C in an oven and an electric grinder to produce the powder of *S. grosvenorii*. The powder was added to 75 % ethanol at a 1:10 (w/v) ratio, thoroughly mixed, and then added to a rotary evaporator for reflux extraction at 60 °C. Filtered and concentrated under decreased pressure to obtain the crude ethanol extract of *S. grosvenorii.*

2.2.2. Crude extract of D. longan pulp

Dried longan pulp obtained from Putian (China), was pulverized by an electric grinder and soaked in 95 % ethanol solution at a ratio of 1:10 (w/v) at room temperature for 12–16 h, and the extraction was repeated 3 times. Filtered and concentrated under reduced pressure to obtain the ethanol crude extract of *D. longan* pulp.

2.2.3. **Crude extract of** *O. stamineus*

The dried *O. stamineus* (Xishuangbanna, China) was crushed with an electric crusher and mixed with 90 % ethanol solution at 1:10 (w/v), and then extracted by reflux in a high-pressure steam extractor at 60 °C. After repeated extraction for 3 times, the crude ethanol extract of *O. stamineu* was obtained by filtering and reducing pressure.

All crude extracts were stored in a refrigerator at 4 °C for the tests described below.

2.3. Total flavonoid content (TFC) and total phenolic content (TPC)

The TPC was performed according to Shahid et al. (2023). 20 µl of Folin-Ciocalteu (FC) reagent was mixed with 70 µl of distilled water and 10 µl of extract (1 mg/ml) in a 96-well plate. After 5 min, 100 µl of NaCO3 (20 %) was added to react in the dark for 30 min. Then, the absorbance was measured at 730 nm in a microplate reader. The TPC was calculated as the gallic acid equivalents (GAE) per gram of extract.

The (TFC) of the extract was estimated by following Salahuddin et al. (2020) method. 30 µl of samples (1 mg/ml), 120 µl of distilled water, and 9 µl of NaNO2 (5 %) were mixed in a 96-well plate. Placed for 5 min, 9 µl of AlCl3 (10 %) was added to react for 5 min. Then, 60 µl of NaOH (1 mol/l) and 72 µl of distilled water were added and the absorbance was measured at 510 nm in a microplate reader. The TFC was expressed as mg of quercetin equivalents (QE) per gram of extract.

2.4. 2,2-Diphenyl-1-picrylhydrazyl (DPPH) radical scavenging activity

The 2,2-Diphenyl-1-picrylhydrazyl (DPPH) radical scavenging activity was determined as previously described (Dappula et al., 2023), with minor modifications. Briefly, in 96-well plates, 50 µl of sample solution and 150 µl of DPPH solution were distributed in each well and incubated overnight at 37C in incubator for 30 mins, and the absorbance of the the sample, trolox, and blank was measured at 517 nm using a microplate reader (Tecan, Switzerland). The percentage of DPPH radical scavenging was calculated through the formula below:

$$Scavenging\ \ activity(\%) = \left(\frac{Absorbance(b) - Absorbance(s)}{Absorbance(b)}\right) \times 100\%$$

$Absorbance(b)$ is the absorbance of the blank and $Absorbance(s)$ is the absorbance of the sample.

2.5. In vitro enzyme inhibition assays

2.5.1. α-Amylase inhibition assay

The iodine starch method with a slight modification was used to evaluate the inhibition of extracts on α-amylase in 96-well plates (Perumal et al., 2022). In brief, 50 µl of crude extract was added to 60 µl 0.1 M PBS (pH 6.9), followed by the addition of 20 µl α-amylase (1U/ml) and incubation at 37 °C for 30 min. Add 50 µl of starch (0.25 %) into the mixture and re-incubate for 15 min. To stop the enzyme reaction, 20 µl of HCl (1 M) was added to the mixture and incubated in a hot bath at 75 °C for 5 min. After cooling to room temperature, 50 µl of iodine reagent was added and absorbance was measured at 620 nm using a microplate reader. DMSO was used as a negative control and acarbose as a positive control. 50 µl crude extract and 200 µl of DMSO were used as blanks.

$$Inhibition(\%) = \left(1 - \frac{Absorbance(N)}{Absorbance(S)}\right) \times 100\%$$

$Absorbance(N)$ is the absorbance of the negative control, and $Absorbance(S)$ is the absorbance of the sample − absorbance of the blank sample.

2.5.2. α-Glucosidase inhibition assay

The α-glycosidase inhibition assay was based on the method described previously with slight modifications (Rakariyatham et al., 2020). Briefly, the extracted samples were diluted to six concentration gradients, and then 10 µl the diluted sample, 130 µl 50 mM PBS (pH 6.5), and 10 µl α-glucosidase (1.5 U/ml) were mixed in a 96-well microplate. The mixture was incubated at 37 °C for 30 min. Then, 50 µl 1 mM *p*-nitrophenyl-α-D-glucopyranoside (PNPG solution) was added and incubated at the same temperatures and re-incubated at the same temperatures. Finally, 50 µl 0.2 M Na_2CO_3 was added to terminate the reaction. The absorbance was measured using a microplate reader (Tecan, Switzerland) at 405 nm. Acarbose was used as a positive control, and DMSO was used as a negative control. Each sample and other reagents without the enzyme mixture were used as the blanks. The inhibitory activity of α-glucosidase was determined by using the following formula:

$$Inhibition(\%) = \left(\frac{Absorbance(N) - Absorbance(S)}{Absorbance(N)}\right) \times 100\%$$

Absorbance(N) is the absorbance of the negative control − absorbance of blank negative control. *Absorbance*(S) is the absorbance of the sample - absorbance of the blank sample.

2.5.3. Dipeptidyl dipeptidase enzyme (DPP-4) inhibition assay

The DPP-4 inhibitory activity of the extracts was detected by the DPP-4 inhibitor screening assay kit (MAK203, Sigma-Aldrich, Germany) (Chaipoot et al., 2022). The determination is performed according to the protocol. 49 μl of DPP4 assay buffer and 1 μl of DPP4 enzyme were used to prepare the inhibition reaction mixes. Then, 25 μl of sample mixed with 50 μl of inhibition reaction mixes was incubated at 37 °C for 10 min. After that, 25 μl of enzymatic reaction mix was added to each reaction well and measured the fluorescence with a microplate reader in kinetic mode for 15–30 min at 37 °C.

2.6. Cytotoxic activity of extract on cell lines

2.6.1. Cell culture

The cell culture protocol of L6 rat skeletal muscle (myoblast) cells was carried out according to previous studies (Liu et al., 2021). The was obtained from the Chinese Type Culture Collection (CTCC). The cells were added to DEME with 10 % Fetal bovine serum (FBS), 1 % penicillin, and 1 % streptomycin and cultured in an incubator at 37 °C with a supply of 5 % CO_2.

2.6.2. Cell cytotoxicity

To assess the cytotoxicity of the sample to L6 (myoblast) cells, the CCK- 8 kit (Sigma-Aldrich) was used to detect cell viability (Chen et al., 2022). Briefly, the cells were incubated with 1×10^5 /ml in a 96-well microplate at 37 °C. Samples with different concentrations were treated in the cells and incubated for 24 h, 48 h, and 72 h, respectively. Then, 10 μl of CCK-8 solution was added to each well and incubated for 1 h. The absorption value was determined using a microplate reader at 450 nm.

2.7. 2-NBDG glucose uptake assay

The induction of L6 cell differentiation has been modified according to previous methods (Perumal et al., 2022). In 96-well plates, L6 cells in the logarithmic growth stage were seeded and cultured in 10 %FBS DMEM. After 48 h, the medium was changed to 2 % FBS for differentiation culture, and the medium was changed every 48 h until the differentiation was completed.

The 2-NBDG Glucose Uptake Assay kit (ab235976, Abcam) was used to detect glucose uptake (Moens et al., 2022). According to the manufacturer's protocol, the medium of the differentiated cells was replaced with a glucose-free medium, and the samples were incubated with the cells for 45 min. Then, the diluted 2-NBDG (100–200 μg/ml) was added to each well and incubated at 37 °C for 10 min. The plates were centrifuged at 400*g* for 5 min. After the supernatant was removed, 200 μl of cell-based assay buffer was added to each well. Fluorescence intensity was detected using a flow cytometer (BeamCyte-1026) and calculated using Flowjo 10.8.1 software. 100 nM of insulin was used as positive control and DMSO was used as blank.

The percentage of glucose uptake in the L6 muscle cells was measured according to the following formula:

$$\text{Percentage of glucose uptake } (\backslash\%) = \frac{\text{Fluorescence (Sample)}}{\text{Fluorescence (Blank)}}$$

2.8. Phytochemical analyses by HPLC-MS

The compounds in the extracts were analyzed by the Agilent 1260 UPLC / 6540 Q-TOF with an SB-C18 column (150 mm × 4.6 mm × 5 μl). The solvent gradient consisted of methanol (solvent A) and water (solvent B). Samples were eluted into the electrospray ionization (ESI) mode with a mobile phase flow rate of 1 ml/min, and the column was maintained at 30 °C. The ionization mode gradient elution procedure: 0–25 min, 20–100 % solvent A; 25–30 min, 100–0% solvent A.

2.9. Polyherbal combination of S. grosvenorii, D. longan, and O. stamineus

The activities of each individual crude extract were first detected, and then the combination was mixed in equal proportions (1:1:1 or 1:1) at the same concentration. The same method was used to detect the activity of the combination group.

2.10. In silico studies

2.10.1. Preprocessing of ligands and proteins

From the PubChem database (https://pubchem.ncbi.nlm.nih.gov/) to download all SDF file (2D structure) of the active ingredient identified by LCMS, and then use the LigPrep module in Schrodinger software to process these files and generates 3D chiral conformation. The crystal structure of the α-amylase protein (PDB ID: 3DHP) and DPP-4 protein (PDB ID: 6B1E Chain A) from the RCSB PDB database (https://www.rcsb.org/). The Protein Preparation Wizard module in Schrodinger software was used to protein preprocess, regenerate states of native ligands, H-bond assignment optimization, protein energy minimization, and remove water.

2.10.2. Molecular XP docking and MM-GBSA calculation

The Schrodinger Maestro 13.5 was used for molecular docking. Before molecular docking, using the SiteMap module in Schrodinger to predict the binding site of α-amylase protein, and the Receptor Grid Generation module is then used to set the most suitable Enclosing box to perfectly wrap the predicted binding site. On this basis, the active sites of proteins were obtained. Each ligand was sequentially docked with the active site of the target protein by Glide XP, respectively. The binding sites were visualized by Maestro.

The prime module of Maestro 13.5 was used to determine the MM-GBSA binding energy of the ligand-receptor complex for optimal docking (Basnet et al., 2023). The implicit VSGB solvation model and OPLS4 force field were employed to calculate the binding energy.

2.10.3. Lipinski parameters and ADMET analysis

The QikProp module of Schrodinger software was used to analyze the ADME/T properties (Hussain et al., 2023), and the properties evaluated included hydrophobicity and hydrophilicity (QPlogPo/w, QPPCaco, *etc.*), human oral absorption (%), molecular weight (MW), solubility (QPlogS), total solvent accessible surface area (SASA), *etc*. Then, filter these compounds according to Lipinski's Rule of Five (Hajji et al., 2022).

2.10.4. Molecular dynamics simulations

To further optimize the binding mode of protein-peptide complexes, the Desmond program in Schrodinger Maestro 13.5 was used for conventional molecular dynamics simulation. To parameterize the protein and small molecules, the opls2005 force field was used, while the TIP3P model was applied to the water solvent. The protein-small molecule complex was dissolved in a water cube. the charge of the system was neutralized by adding 0.150 M chloride and sodium ions. Initially, the steepest descent minimization method was used to minimize the system energy for 50,000 steps. Gradually, the positions of heavy atoms were restrained for NVT and NPT equilibration for an additional 50,000 steps. The system pressure and temperature were maintained at 1 bar and 300 K, respectively. After completing the two equilibration stages, an unrestricted simulation was performed for 100 ns. The interactions were then analyzed, and dynamic trajectory animations were generated using

Table 1
Total phenolic content and total flavonoid content.

Sample	Total flavonoid content (TFC) (mg QE /g)	Total phenolic content (TPC) (mg GAE /g)
O. stamineus (OS)	6.12 Â ± 0.35 [a]	9.38 Â ± 0.62[a]
S. grosvenorii (SG)	0.75 Â ± 0.23[c]	1.35 Â ± 0.10c
D. longan (DL)	0.15 Â ± 0.05 [c]	0.73 Â ± 0.02[c]
SG + DL + OS	4.03 Â ± 0.27[b]	6.04 Â ± 0.41[b]
SG + OS	3.92 Â ± 0.58[b]	5.88 Â ± 0.21[b]
DL + OS	3.61 Â ± 0.36[b]	5.60 Â ± 0.11[b]
SG + DL	0.49 Â ± 0.08[c]	1.11 Â ± 0.09[c]

Values are mean ± standard deviation of triplicate determination. Different superscript letters in each row indicate that values are significantly different ($P < 0.05$). GAE: Gallic acid equivalent; QE: Quercetin equivalent. Values are mean ± standard deviation.

Schrodinger Maestro 13.5.

2.11. Statistical analysis

SPSS 21 and GraphPad Prism 9 were used for statistical analysis. The outcomes were expressed as mean ± standard deviation (SD) and used analysis of variance (ANOVA) followed by Dunnett's *t*-test (GraphPad Prism 9). Probability values of $p < 0.05$ were considered significant. The IC_{50} was determined using GraphPad Prism 9.

3. Results and discussion

3.1. Estimation of total phenolic content (TPC) and flavonoid content (TFC)

Plant extracts are known to contain a diverse array of non-nutritional substances, referred to as phytochemicals or nutraceuticals, which have the potential to confer a range of health advantages. Among these different types of phytochemicals, phenolic compounds are widely acknowledged as the primary agents responsible for antioxidant activity. These compounds exhibit a diverse range of effects, including antioxidant, antibacterial, anti-inflammatory, and other properties (Mohamed et al., 2022), and are being widely used in many industries, such as food, pharmaceuticals, and health products. Flavonoids constitute a significant class of secondary plant metabolites that possess diverse biological activities both *in vivo* and *in vitro*, particularly in terms of their antioxidant capabilities (Bibi et al., 2022).

The Folin Ciocalteu method and the Aluminium Chloride Colorimetric method were employed to quantify total phenolic content (TPC) and total flavonoid content (TFC) in each sample according to the standard curve formula of gallic acid and quercetin, respectively. The results showed (Table 1) that under the same ratio, the combination of *SG + DL + OS* had the highest TPC and TFC, with values of 6.04 ± 0.41 mg GAE/g and 4.03 ± 0.27 mg QE/g, respectively. In contrast, the lowest TPC and TFC of the combination of *SG + DL* were 1.11 ± 0.09 mg GAE/g and 0.49 ± 0.08 mg QE/g, respectively. The other two combinations, *SG + OS* contain 5.88 ± 0.21 mg GAE/g and 3.92 ± 0.58 mg QE/g, and *DL + OS* contain 5.60 ± 0.11 mg GAE/g and 3.61 ± 0.36 mg QE/g, respectively.

The TPC and TFC in the *D.longan* extract were found to be the lowest among the three individual crude extracts, with TPC measuring 0.73 ± 0.02 mg GAE/g and TFC measuring 0.15 ± 0.05 mg QE/g. Nevertheless, the extract of *O. stamineus* exhibited the highest TPC with a value of 9.38 ± 0.62 mg GAE/g, as well as the highest TFC with a value of 6.12 ± 0.35 mg QE/g. The TPC and TFC of the extracts from *S. grosvenorii* were found to be 1.35 ± 0.10 mg GAE/g and 0.75 ± 0.23 mg QE/g, respectively. Hence, it can be inferred that, when considering the same mixing ratio, the TPC and TFC of the combination including *D. longan* extract will be comparatively lower than other combinations. Conversely, the combination containing *O. stamineus* extract will exhibit a higher content.

3.2. DPPH radical scavenging activity

The DPPH radical scavenging activity is a widely employed approach for assessing antioxidant activity in food and herbal extracts. This method is known for its simplicity, sensitivity, speed, reproducibility, and practicality (Gulcin and Alwasel, 2023).

The DPPH radicals scavenging activities of individual extracts and different combinations are shown in Fig. 1. Overall, each of the combinations exhibited the DPPH scavenging activity, but the effect was less potent compared to Trolox (IC_{50} of 0.54 ± 0.02 mg/ml) and extracts of *O. stamineus* (IC_{50} of 0.92 ± 0.05 mg/ml). In contrast, the DPPH scavenging capacity exhibited by various combinations surpassed that of extracts from *S. grosvenorii* (IC_{50} of 13.84 ± 0.94 mg/ml) and *D. longan* (IC_{50} of 22.58 ± 0.93 mg/ml). The synergistic impact of the combination of *SG + DL + OS* demonstrated superior efficacy in the scavenging

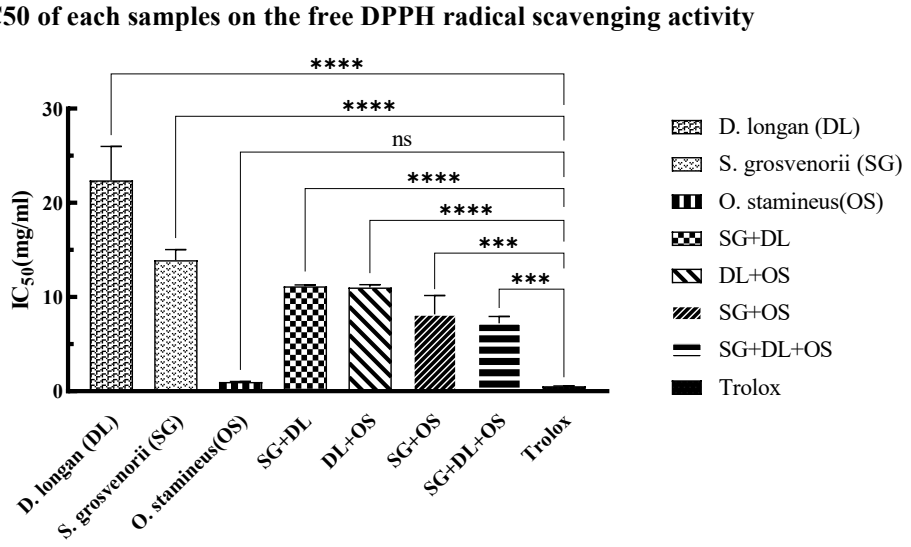

Fig. 1. The IC_{50} of different samples on the free DPPH radical scavenging activity. Values are mean ± standard deviation of triplicate determination. The difference * shows a significant ($p < 0.05$) difference between various samples and Trolox, *< 0.05, **< 0.01, ***< 0.005, ****< 0.0001.

Table 2
The α-glucosidase and α-amylase inhibitory activities.

Sample	α-Glucosidase inhibition, IC_{50} (mg/ml)	α-Amylase inhibition, IC_{50} (mg/ml)
D. longan (DL)	45.90 ± 0.78^{a}	38.04 ± 0.82^{a}
S. grosvenorii (SG)	12.94 ± 0.71^{b}	22.34 ± 0.16^{b}
O. stamineus (OS)	4.71 ± 0.14^{cd}	13.23 ± 0.26^{cd}
SG + DL	9.66 ± 0.74^{c}	16.33 ± 0.87^{bc}
DL + OS	9.06 ± 0.13^{cd}	11.16 ± 0.44^{de}
SG + OS	3.61 ± 0.72^{d}	7.27 ± 0.11^{e}
SG + DL + OS	5.41 ± 0.67^{cd}	8.63 ± 0.35^{de}
Acarbose	0.0053 ± 0.0003^{e}	0.0478 ± 0.013^{f}

Values are mean ± standard deviation of triplicate determination. Different superscript letters in each row indicate that values are significantly different ($P < 0.05$).

of free radicals, as evidenced by the much lower IC_{50} value of 7.21 ± 0.72 mg/ml. The IC_{50} value of the *SG + DL* group had the highest, measuring at 11.16 ± 0.14 mg/ml. This was followed by the combination of *DL + OS* and *SG + OS* with IC50 values of 8.17 ± 0.77 mg/ml and 10.93 ± 0.30 mg/ml, respectively.

3.3. The α-glucosidase and α-amylase inhibitory activities

The enzymes α-glucosidase and α-amylase play crucial roles in the metabolic processes of dietary carbohydrates. Competitive inhibitors of these enzymes can manage blood sugar levels by delaying carbohydrate digestion and reducing the rate of glucose absorption. At present, the α-glucosidase and α-amylase inhibitors have been shown to be one of the effective strategies for the treatment of T2DM (Huneif et al., 2022). In this study, the individual extract was mixed in equal proportions according to its IC_{50} to form different combinations, and then the α-glucosidase and α-amylase inhibitory activities of the combined group were tested by the same method, and Acarbose was employed as the control. The results of the α-glucosidase and α-amylase inhibition of various combinations are presented in Table 2.

Based on the findings from the test results, among the individual extracts, it can be observed that the extract of *O. stamineus* shows the best inhibitory capacity on the two enzymes by compared to the other individual extracts, and its IC_{50} values were 4.71 ± 0.14 mg/ml (α-glucosidase) and 13.23 ± 0.26 mg/ml (α-amylase), respectively. Subsequently, the extract of *S. grosvenorii* demonstrated an IC_{50} value of 12.94 ± 0.71 mg/ml for α-glucosidase and 22.34 ± 0.16 mg/ml for α-amylase. Conversely, the inhibitory effect of *D. longan* extract was shown to be less potent compared to the aforementioned extracts.

Among different combinations, the highest IC $_{50}$ value of α-glucosidase inhibition was observed in the combination of *SG + DL*, with IC50 of 9.66 ± 0.74 mg/ml, indicating that the α-glucosidase inhibitory ability of this combination was lower than that of other combinations. This is followed by the combination of *DL + OS* and *SG + DL + OS*, the values of IC_{50} are 9.06 ± 0.13 mg/ml and 5.41 ± 0.67 mg/ml, respectively. However, the combination of *SG + OS* exhibited the best inhibitory glucosidase activity, with an IC_{50} value of 3.61 ± 0.72 mg/ml. As a result of α-amylase inhibition (Table 2), the same effect is observed at the same time. From low to high, the IC 50 value of α-amylase inhibition was as follows: *SG + OS* (7.27 ± 0.11 mg/ml) < *SG + DL + OS* (8.63 ± 0.35 mg/ml) < *DL + OS* (11.16 ± 0.44 mg/ml) < *SG + DL* (16.33 ± 0.87 mg/ml).

Above all, based on the inhibitory activity of various combinations on the two enzymes, it was noted that the inhibitory potency of each combination on α-glucosidase was superior to that on α-amylase. The combination of *SG + OS* showed a greater inhibitory effect than other combinations, but the combination of *SG + DL* exhibited the lowest inhibitory effect among the combinations.

3.4. Dipeptidyl peptidase-4 (DPP-4) enzyme inhibitory activities

Dipeptidyl peptidase-4 (DPP4) enzyme is a serine protease that plays a crucial role in glucose and insulin metabolism. Consequently, it has been identified as a key therapeutic target for the treatment of diabetes (Yin et al., 2022). Various combinations were evaluated for their *in vitro* inhibitory activities against DPP-4 by using the fluorescence method.

As depicted in Fig. 2, various combinations exhibit inhibitory effects on the DPP-4 enzyme. Notably, within a certain concentration range, the inhibitory effect of these combinations was superior to 18 nM Sitagliptin (52.24 ± 0.18 %, inhibition rate) and 5ug/ml insulin (56.06 ± 0.24 %, inhibition rate). Furthermore, the degree of inhibition was directly proportional to the concentration of the drug combination. Additionally, it was also found that, at equivalent concentrations, the individual crude of *S. grosvenorii (SG)* and *D. longan (DL)* had no inhibitory effect on the DPP-4 enzyme. Simultaneously, the combination of *SG + DL + OS* (2.894 ± 0.094 mg/ml, IC_{50}) and *DL + OS* (1.199 ± 0.073, IC_{50}) exhibited a superior inhibitory action compared to the individual crude of *O. stamineus (OS)* with IC_{50} value of 3.742 ± 0.388 mg/ml. However, the combination of *SG + OS* showed the highest IC_{50} of 4.432 ± 0.272 mg/ml. The results indicate that *O. stamineus (OS)* extract plays an important role in the anti-DPP-4 enzyme activity of multidrug combinations.

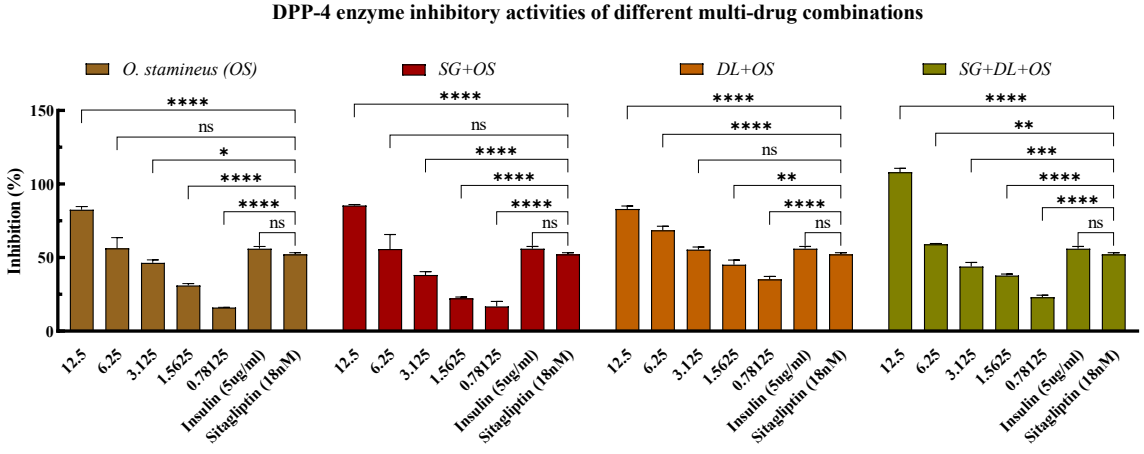

Fig. 2. Inhibitory activity of DPP-4 enzyme. Values are mean ± standard deviation of triplicate determination. The difference * shows a significant ($p < 0.05$) difference between various combinations with different concentrations and Sitagliptin (18 nM), *ns: not significant, * < 0.05, ** < 0.01, *** < 0.005, **** < 0.0001*.

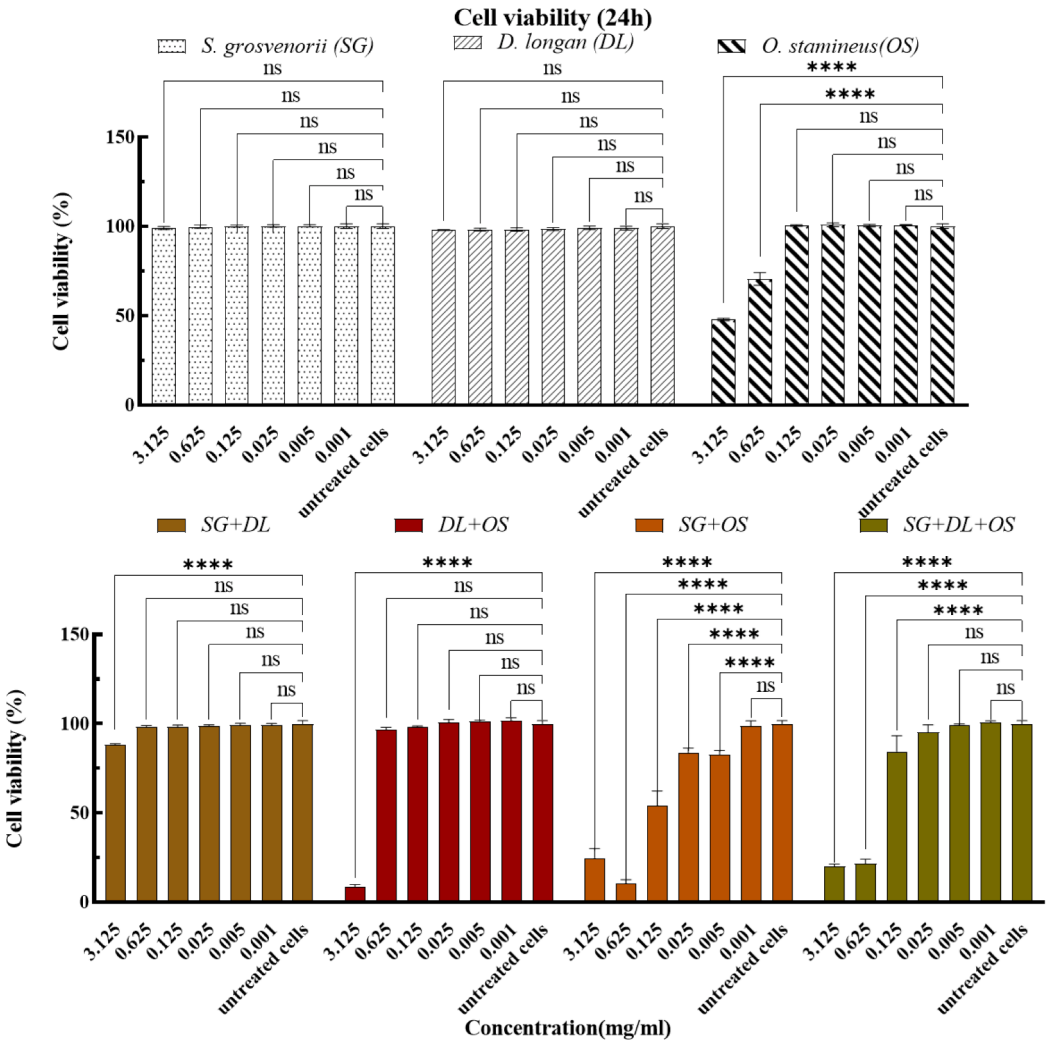

Fig. 3. The effects of various combinations after 24 h treatment on cell viability. Values are mean ± standard deviation of triplicate determination. The difference * shows a significant ($p < 0.05$) difference between untreated cells and treated cells by various combinations with different concentrations, *ns: not significant, * < 0.05, ** < 0.01, *** < 0.005, **** < 0.0001.*

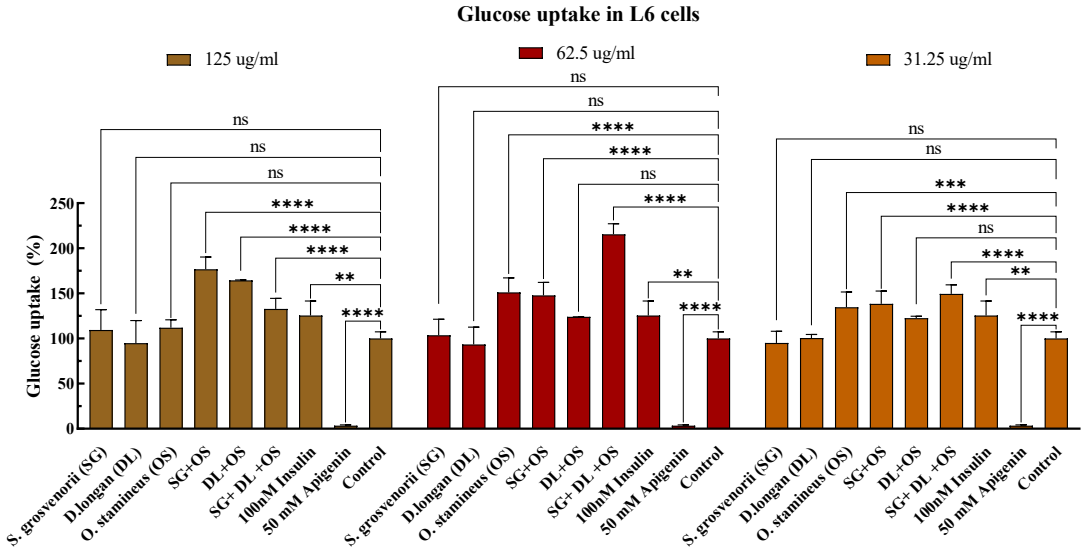

Fig. 4. Effect of various combinations on glucose uptake. Values are mean ± standard deviation of triplicate determination. The difference * shows a significant ($p < 0.05$) difference between untreated cells and treated cells, *ns: not significant, * < 0.05, ** < 0.01, *** < 0.005, **** < 0.0001.*

Table 3
ADMET properties and physico-chemical properties using Lipinski's five rules.

Compd. No	MW	SASA	QPlogPo/w	QPlogS	QPlogHERG	QPPCaco	QPlogBB	QPlogKhsa	% HOA	No. of violation
1	346.293	571.719	1.299	−3.545	−4.964	57.578	−2.030	−0.139	66.057	0
2	250.254	480.454	−0.337	−1.467	−4.649	173.111	−1.545	−0.887	65.034	0
3	270.241	490.890	1.606	−3.344	−5.161	117.545	−1.445	−0.043	73.403	0
4	281.271	483.525	−1.073	−1.770	−3.827	97.320	−1.528	−0.857	56.246	0
5	208.300	422.827	2.731	−2.962	−2.867	3922.673	0.184	0.154	100.000	0
6	168.198	372.242	2.319	−2.487	−4.433	3208.060	0.152	−0.077	100.000	0
7	308.293	556.829	2.305	−3.970	−3.934	45.367	−1.388	−0.193	70.096	0
8	330.293	557.630	1.851	−3.749	−4.956	124.627	−1.606	0.004	75.289	0
9	313.331	518.447	−1.779	−0.599	−4.199	1.494	−1.961	−1.049	19.651	0
10	311.507	725.287	2.791	−5.174	−4.049	45.109	−1.210	0.508	72.894	0
11	226.234	466.178	2.373	−3.559	−5.056	1101.064	−0.401	0.064	95.285	0
12	313.352	624.465	2.793	−4.211	−6.024	304.601	−1.622	0.055	87.755	0
13	309.491	624.883	4.033	−3.768	−4.777	1231.753	0.302	0.601	100.000	0
14	281.271	483.753	−1.139	−1.772	−3.838	93.851	−1.561	−0.874	55.581	0
15	168.198	372.923	2.321	−2.499	−4.462	3215.965	0.152	−0.077	100.000	0

Note: Compd. No 1: 5,3′,4′,5′-Tetrahydroxy-6,7-dimethoxyflavone; 2: 80840-09-1; 1-(2-Quinoxalinyl)-1,2,3,4-butanetetrol; 3: apigenin; 4: 2′-O-Methyladenosine; 5: CHEBI:167940; 6: HARMINE; 7: Flazin; 8: Quercetin 3,4′-dimethyl ether; 9: Methylthioadenosine sulfoxide; 10: 13-Azaprostanoic acid; 11: beta-Carboline-3-carboxylic acid methyl ester; 12: N-Trans-feruloyltramine; 13: Dicyclomine; 14: 2′-O-Methyladenosine; 15: Tetrahydroharman-3-carboxylic acid.
MW: Molecular weight (≤500 Da); SASA: Total solvent accessible surface area; QPlogPo/w: Partition coefficient (−2 to 5); QPlogS: Water solubility (−5 to −0.5); QPlog HERG: Prediction of blockade of HERG K^+ channels (> −5); QPP Caco: Permeability across gut in nm/s (< 25 (poor), > 500 (excellent)); Log BB: Brain/blood partition coefficient (−3 to 0.5); QPLog Khsa: Binding to human serum albumin (-0.5 to 1); % HOA: Human oral absorption (0–100 %); No. of violation: Number of violations of Lipinski's five rules.

3.5. Cytotoxic activity on L6 cell lines

The cytotoxicity of the various combinations was investigated on L6 cell lines by using the wells without cells and containing medium and the CCK-8 solution was blank. The negative control was untreated cells. From the CCK-8 assay results presented in Fig. 3, the individual crude extracts of *S. grosvenorii* and *D. longan* had no effect on cell viability at the set concentration. However, the individual crude extracts of *O. stamineus* and the combination group had effects on cell viability, and it was found that the viability of L6 cells gradually decreased as the concentration increased. When the treatment time was 24 h, the combination of *SG* + *DL* had little on L6 cell viability, while the other three groups had a greater influence on the viability of L6 cells at higher concentrations. Based on the value of IC_{50} in cytotoxic, the combination of *SG* + *OS* had the most potent cytotoxic activity, its IC_{50} was 0.1343 ± 0.028 mg/ml. This is followed by the combination *SG* + *DL* + *OS and* the combination *DL* + *OS*, the IC_{50} is 0.3241 ± 0.047 mg/ml and 1.604 ± 0.065 mg/ml, respectively. In addition, the IC_{50} of the individual crude extracts of *O. stamineus* on cytotoxicity was 2.541 Â ± 0.019 mg/ml. According to the results, the impact of the combination *SG* + *DL* + *OS, DL* + *OS* and *SG* + *OS* on cell viability is higher than the individual crude extracts of *O. stamineus*, and it can be inferred that under the same concentration conditions, the inhibitory effect of the combination group on cell proliferation may be better than the individual crude extracts.

3.6. 2-NBDG glucose uptake assay on L6 cell lines

Assay on glucose uptake study on L6 cell lines was assessed by using the 2-NBDG Glucose kit. In this study, based on the detection results of cell viability, each group with concentrations at 125 ug/ml, 62.5 ug/ml, and 31.25 ug /ml (more than 70 % of living cells) was selected for glucose uptake detection. Untreated cells and cells treated with 100 nM insulin were used as positive control, and cells treated with 50 mM Apigenin were used as the negative control.

The results clearly showed that the *O. stamineus* extracts could boost the glucose uptake of L6 myoblasts at various concentrations, but the *S. grosvenorii* and *D. longan* extracts had no discernible impact (Fig. 4). Various combinations-treated L6 cells significantly ($P < 0.05$) boost glucose uptake, as shown in Fig. 4. Compared with untreated cells, the glucose uptake rates of the combination *SG* + *OS*, *DL* + *OS*, and *SG* + *DL* + *OS* at 31.25ug/ml were 138.39 %, 149.43 %, and 122.53 %, respectively. The combination *SG* + *DL* + *OS* showed the highest glucose uptake capacity at 62.5ug/ml, up to about 215.55 %, and the combination *SG* + *OS* and *DL* + *OS* showed 136.47 % and 123.96 %, respectively. On the contrary, the combination *SG* + *OS* and *DL* + *OS* showed higher glucose uptake at high concentrations (125ug/ml), with an uptake rate of 159.50 % and 164.56 % respectively, while the combination *SG* + *DL* + *OS* showed a lower uptake rate of 132.88 %.

3.7. Identification of bioactive constituents by HPLC/ LC-MS

The HPLC/ LC-MS technique was used to identify the bioactive components of the crude extracts of *S. grosvenorii, D. longan,* and *O. stamineus*. After database annotation, the bioactive compounds were preliminarily identified. These compounds were used *in silico* analysis.

3.8. In silico studies

Its potential anti-diabetic was further studied by molecular docking and dynamic simulation, the human salivary α-amylase (3DHP) and DPP-4 (6B1E Chain A**)** were used as the target protein.

3.8.1. Molecular XP docking and MM-GBSA calculation

Extra-Precision (XP) docking method, also known as flexible docking, is the most refined computing mode that can be used to perform higher-resolution molecular docking calculations on specific targets. The XP docking is time-consuming, but its results have higher accuracy and reliability (Baby et al., 2023). In general, when XP Gscore is less than −6, it indicates that the binding between ligand and ligand–protein is stable. According to the XP docking results, with the XP Gscore ≤-6 as the screening criteria, 336 compounds, and 306 compounds can form relatively stable binding with α-amylase protein (3DHP) and DPP-4 protein (6B1E Chain A), respectively, and these compounds will be used for subsequent MM-GBSA analysis. The results of XP docking and MM-GBSA analysis are shown in Table A.1 as supplementary materials.

Based on the outcomes of XP docking, compounds with XP Gscore ≤ -6 were selected for MM-GBSA analysis. When MM-GBSA dG Bind value is less than −30 kcal/mol, it indicates that the binding between ligand and protein is stable. According to the analysis results of MM-GBSA of the two target proteins, 26 and 32 compounds were found to meet the criteria, respectively. The XP Gscore and MM-GBSA binding free energy of these ligand compounds are shown in Table B.1 as supplementary

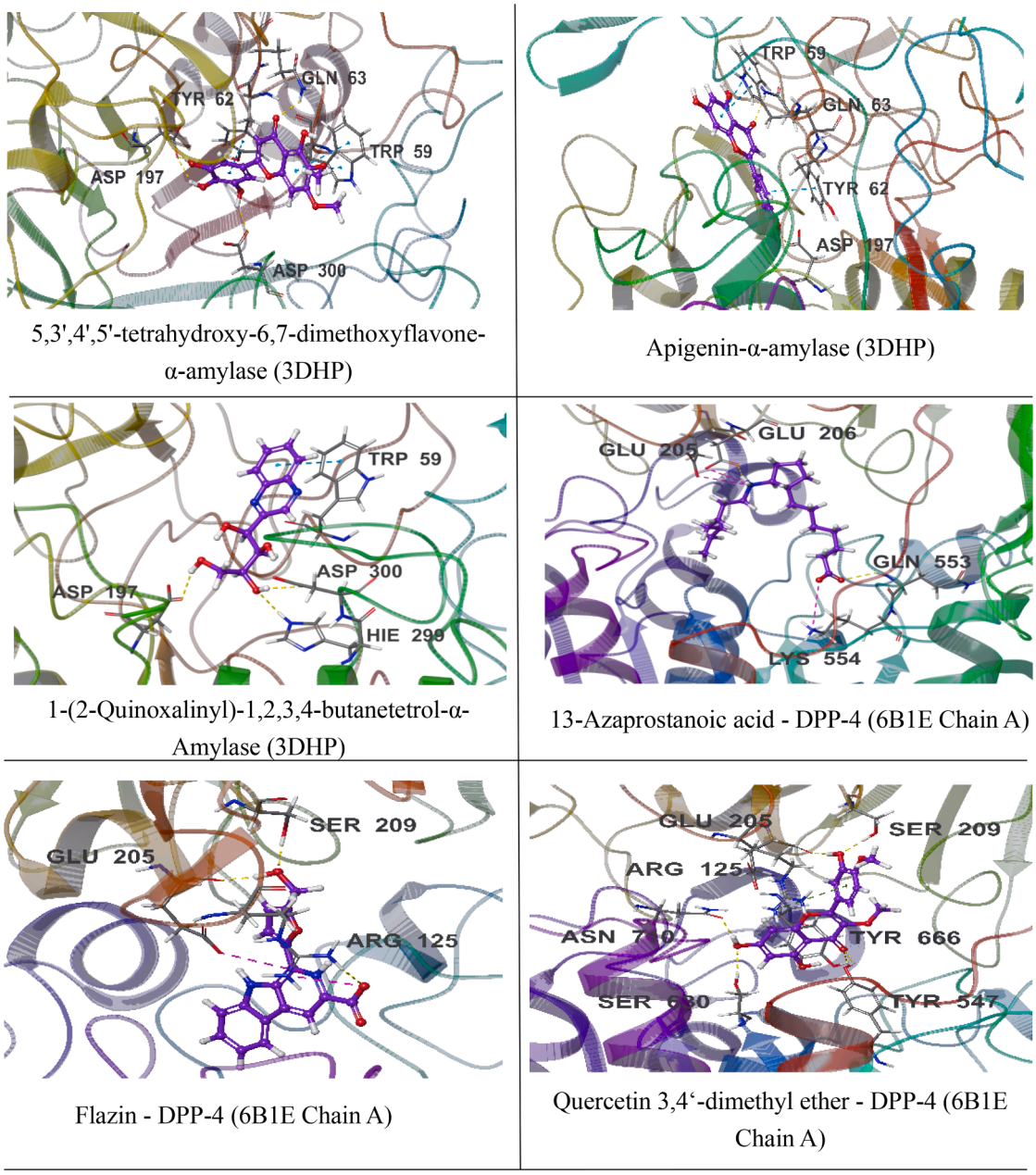

Fig. 5. 3D docking interaction of 3 compounds with α-amylase (3DHP) protein and DPP-4 (6B1E Chain A) protein.

materials.

3.8.2. Determination of Lipinski parameters and ADMET analysis in silico

To predict the bioavailability and toxicity of screened compounds, the evaluation of properties related to absorption, distribution, metabolism, excretion, and toxicity (ADMET) is considered more important (Bhakhar et al., 2021). We use Schrodinger's QikProp module for ADME/T analysis of ligand compounds screened from XP GScore and MM-GBSA, which are mainly evaluated with reference to the Lipinski five rules. The molecules that conform to Lipinski's five rules and properties of molecules are shown in Table 3.

A total of 15 molecules perfectly conform to Lipinski's five rules. From the values of logS and QPP Caco, we can predict that these compounds have better water solubility and intestinal cell permeability. For QPlogBB, negative values indicate that the compound is polar and has poor blood–brain barrier permeability, and the values of these compounds all have extremely poor permeability, indicating minimal risk of central nervous system toxicity. It was also observed that the oral absorption rate of these molecules was higher than 50 %, indicating that the oral route could be used as a mode of administration. Overall, these compounds have good ADMET properties and do not show violations of Lipinski's five rules, suggesting that they are suitable as candidate combinations for anti-diabetic potential.

Fig. 5 shows the interactions of each 3 compounds (the compounds with the best XP Gscore and MM-GBSA binding free energy, selected from 15 compounds that conform to Lipinski's five rules) with α-amylase (3DHP) protein and DPP-4 (6B1E Chain A) protein via XP docking (3D). 5,3′,4′,5′-tetrahydroxy-6,7-dimethoxyflavone binds to the surface of α-amylase (3DHP) and forms hydrophobic forces with residues ALA198, TYR62, TRP59, TRP58, and LEU16, forms one hydrogen bond with residues ASP300 and GLN63, two hydrogen bonds with residues ASP197, one π-π bond with residues TYR62, and two π-π bonds with residues TRP59. Apigenin binds to the surface of α-amylase (3DHP) and forms hydrophobic forces with residues ALA198, TYR62, TRP59,

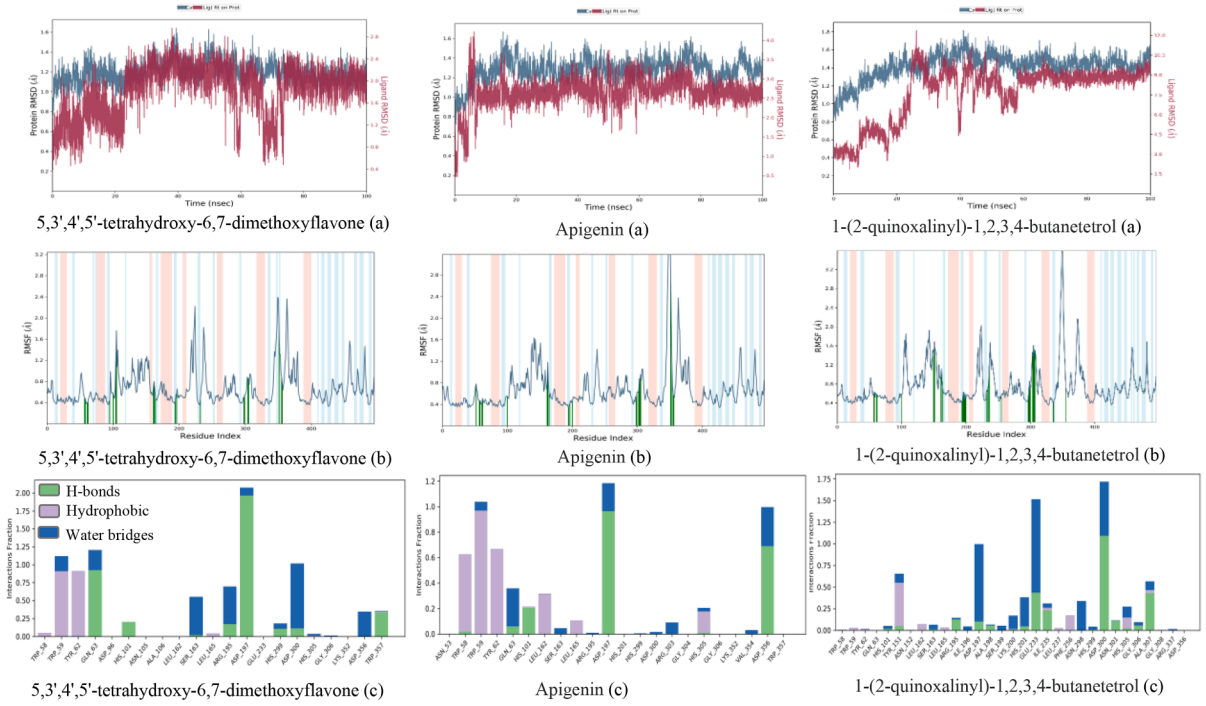

Fig. 6. The RMSD (a), RMSF (b) trajectories and interaction (c) of α-amylase (3DHP) protein–ligand (ligands: 5,3′,4′,5′-tetrahydroxy-6,7-dimethoxyflavone, apigenin, and 1-(2-quinoxalinyl)-1,2,3,4-butanetetrol).

TRP58, and LEU16, forms one hydrogen bond with residues ASP197 and GLN63, forms a π-π bond with residues TYR62 and forms two π-π bonds with residues TRP59. 1-(2-Quinoxalinyl)-1,2,3,4-butanetetrol-α-Amylase (3DHP): 1-(2-quinoxalinyl)-1,2,3,4-butanetetrol binds to the surface of α-amylase and forms hydrophobic forces with residues TYR62, LEU162, TRP59, TRP58, LEU16, forms a hydrogen bond with residues HIE299, ASP300, and ASP197, and a π-π bond with residues TRP59.

13-Azaprostanoic acid - DPP-4 (6B1E Chain A): 13-Azaprostanoic acid penetrates deep into the active pocket of DPP-4 protein, forming hydrophobic forces with residues VAL711, VAL656, TRP659, TYR631, PHE357, and forming a hydrogen bond with residues GLN553. Forming a salt bridge with residues LYS554 and GLU205, and forming a hydrogen bond and a salt bridge with residues GLU206. Flazin - DPP-4 (6B1E Chain A): Flazin penetrates deep into the active pocket of DPP-4 protein, forming hydrophobic forces with residues TYR662, TYR666, TRP659, VAL656, TYR631, forming a hydrogen bond with residue SER209, and forms a hydrogen bond and a salt bridge with residues GLU205 and ARG125. Quercetin 3,4‘-dimethyl ether - DPP-4 (6B1E Chain A): Quercetin 3,4‘-dimethyl ether penetrates deep into the active pocket of DPP-4 protein, forming hydrophobic forces with residues PHE357, TYR666, TYR547, TYR631, forming a hydrogen bond with residues SER209, GLU205, ASN710, SER630, TYR547, TYR666, and a π-cation bond with residues ARG125.

3.8.3. *Molecular dynamics simulations*

Molecular dynamics (MD) simulation is an important computational tool for evaluating the time-dependent stability of ligands entering the active site of the receptor complex (Gajjar et al., 2021). To further optimize the binding pattern of the ligand–protein complex, a 100 ns unrestricted simulation was conducted using the Desmond program. Furthermore, the interactions and dynamic trajectory animations were analyzed using Maestro 13.5. The results of MD simulations were evaluated using plots such as root mean square deviation (RMSD), root mean square fluctuation (RMSF), radius of rotation (rGyr), intramolecular hydrogen bond (introHB), solvent accessible surface area (SASA), and molecular surface area (MolSA).

3.8.3.1. MD simulation of ligand-α-amylase (3DHP) protein. MD simulations of 5,3′,4′,5′-tetrahydroxy-6,7-dimethoxyflavone, apigenin, and 1-(2-quinoxalinyl)-1,2,3,4-butanetetrol with α-amylase (3DHP) protein were simulated by 100 ns to analyze the molecular dynamics trajectories.

Based on the study of root mean square deviation (RMSD) for conformational stability during the simulation period, it can be observed that the complexes attained stable conformations as evidenced by the presence of small fluctuations. The results of RMSD (a) (Fig. 6) showed that 5,3′,4′,5′-tetrahydroxy-6,7-dimethoxyflavone, apigenin, and 1-(2-quinoxalinyl)-1,2,3,4-butanetetrol were relatively stable with α-amylase protein after 80 ns, 10 ns, and 60 ns, respectively. And the subsequent fluctuations also gradually stabilized, indicating that the system reached the equilibrium state. The stability of a receptor can be reflected by the analysis of root mean square fluctuation (RMSF) by characterizing the flexibility of each receptor residue. The peak value observed in the RMSF plot corresponds to the residue region that fluctuates the most during the simulation. RMSF (b) (Fig. 6) showed that after 5,3′,4′,5′-tetrahydroxy-6,7-dimethoxyflavone was bound to α-amylase protein, in the residue regions 220-230AA, 240-250AA, 340-350AA, and 350-360AA exhibited high RMSF values, indicating higher structural flexibility in these regions. When apigenin was combined with α-amylase protein, the protein showed high structural flexibility in 145-160AA, 340-350AA, and 360-370AA residue regions. At the same time, when 1-(2-quinoxalinyl)-1,2,3,4-butanetetrol was bound to α-amylase protein, the protein showed high structural flexibility in the 100-110AA, 220-230AA, and 340-350AA residue regions.

Protein-ligand interactions can be monitored throughout the simulation, and their interactions can generally be classified into four types: hydrogen bonding, hydrophobic interaction, lonic, and water bridge. As depicted in Fig. 6 (c), 5,3′, 4′, 5′ -tetrahydroxy −6, 7-dimethoxy-flavonoids interact with the residues RP59 and TYR62, GLN63 and ASP197, and ASP300 of the -amylase protein via hydrophobic interaction, hydrogen-bonding, and the formation of water bridges,

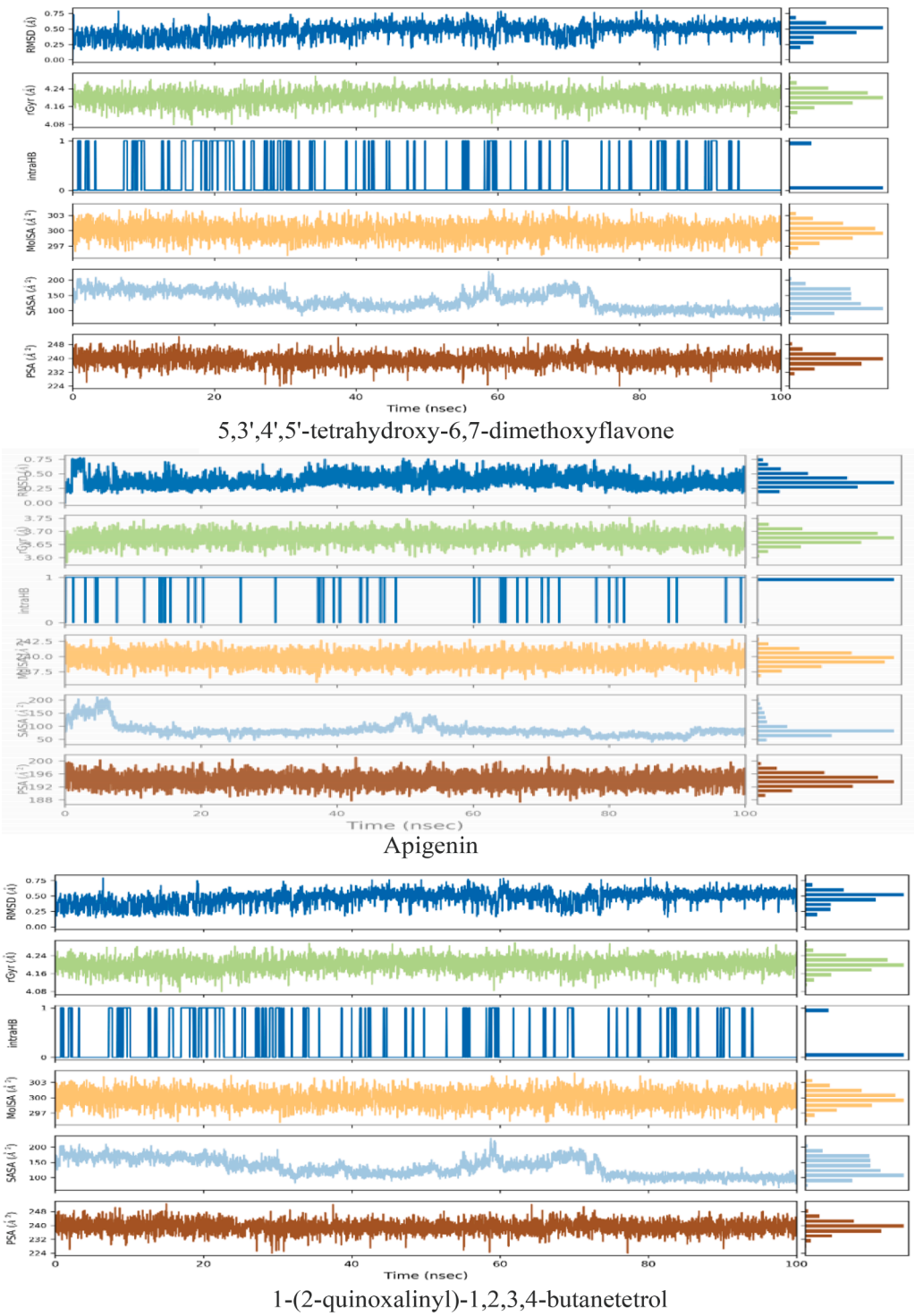

Fig. 7. Variation in the ligands (ligands: 5,3′,4′,5′-tetrahydroxy-6,7-dimethoxyflavone, apigenin, and 1-(2-quinoxalinyl)-1,2,3,4-butanetetrol) properties w.r.t time during the course of 100 ns simulation.

respectively, resulting in their tight association. Apigenin exhibits binding affinity towards α-amylase proteins and engages in interactions with residues, namely TRP58, TRP59, TYR62, ASP197, and ASP35, through the formation of hydrogen bonds and hydrophobic interactions. The residues TYR151, ASP197, GLU233, and ASP300 are crucial in the interaction between the α-amylase protein and 1-(2-quinoxalinyl)-1,2,3,4-butanetetrol. The primary mode of interaction is through the formation of water bridge and hydrogen bonding.

Different parameters were calculated to gain insight into the conformational strains that ligands undergo to maintain protein-binding complexes. rGyr: Characterizes the extension of the ligand. introHB: The number of internal hydrogen bonds (HB) within the ligand molecule. MolSA: equivalent to a van der Waals surface area. SASA: The surface area of a molecule accessible to water molecules. PSA: The surface area of a molecule where only oxygen and nitrogen atoms contribute to the solvent.

As shown in Fig. 7, 5,3′,4′,5′-tetrahydroxy-6,7-dimethoxyflavone, apigenin, and 1-(2-quinoxalinyl)-1,2,3,4-butanetetrol remain basically

constant in RMSD during the simulation. Moreover, in the α-amylase (3DHP) protein receptor binding pocket, the rGyr fluctuations of 5,3′,4′,5′-tetrahydroxy-6,7-dimethoxyflavone, apigenin, and 1-(2-quinoxalinyl)-1,2,3,4-butanetetrol remained almost constant, with rGyr values ranging from 4.08 to 4.24 Å, 3.60–3.75 Å and 4.08–4.24 Å, respectively. It was shown that the ligand was almost steady in 100 ns simulation time. In general, higher MolSA and PSA values contribute to better stability (Chaieb *et al.,* 2022). The MolSA values (Fig. 7) of 5,3′,4′,5′-tetrahydroxy-6,7-dimethoxyflavone, apigenin, and 1-(2-quinoxalinyl)-1,2,3,4-butanetetrol are 297–303 $Å^2$, 237–242 $Å^2$, 297–303 $Å^2$, respectively, and the PSA values (Fig. 7) are 224–248 $Å^2$, 188–200 $Å^2$, and 224–248 $Å^2$, respectively. However, the lower the SASA value, the better the stability of the complex during the simulation (Samad *et al.,* 2022). The results show that the SASA values of the 5,3′,4′,5′-tetrahydroxy-6,7-dimethoxyflavone and 1-(2-quinoxalinyl)-1,2,3,4-butanetetrol are in the range of 100–200 $Å^2$, while the apigenin is in the range of 50–200 $Å^2$. In addition, during the simulation period, the fluctuations of MolSa values, PSA values, and SASA values gradually decreased, indicating that the complex became more stable and compact.

3.8.3.2. MD simulation of ligand - DPP-4 (6B1E Chain A) protein. MD simulations were performed to analyze the steady and stability of ligand-ligand - DPP-4 (6B1E Chain A) protein (ligands: flazin, quercetin 3,4′-dimethyl ether, and 13-azaprostanoic acid) in 100 ns.

The results of RMSD (a) (Figure C.1) showed that flazin, quercetin 3,4′-dimethyl ether, and 13-azaprostanoic acid were relatively stable with DPP-4 (6B1E Chain A) protein after 30 ns, 40 ns, and 10 ns, respectively, and the system was in equilibrium. Furthermore, the flazin-DPP-4 protein complex exhibits RMSD fluctuation range of 1.00–1.80 Å, while the RMSD fluctuation range of the quercetin 3,4′-dimethyl ether-DPP-4 complex is 1.00–2.00 Å. The RMSD value of 13-azaprostanoic acid-DPP-4 fluctuated in the range of 0.75–2.00 Å. Typically, ligand–-protein complexes with less deviation are more stable. Hence, it can be observed that the stability of ligand 13-azaprostanoic acid towards DPP-4 protein is rather low in comparison to the other two ligands. RMSF (b) (Figure C.1) showed that after flazin was bound to DPP-4 protein, the protein showed high structural flexibility in the residue regions of 200-220AA, 240-250AA, and 485-500AA. When quercetin 3,4′-dimethyl ether was combined with DPP-4 protein, the protein showed high structural flexibility in 200-220AA and 240-250AA residue regions. At the same time, when 13-azaprostanoic acid was bound to the DPP-4 protein, the protein showed high structural flexibility in the 200-220AA and 240-250AA residue regions.

As shown in Figure C.1 (c), the residues PHE357, ARG358, TYR547, and GLN553 play an important role in flazin and DPP4 protein binding. Amino acid residues that quercetin 3,4′-dimethyl ether combined with DPP4 protein were TYR547, CYS551, GLN553, and LYS554. In addition, the GLU206, GLN553, LYS554, and TYR666 play an important role in 13-azaprostanoic acid and DPP4 protein binding. Their interactions are mainly hydrogen bonding, water bridge, and hydrophobic.

From simulation trajectories (Figure C.2), in the DPP-4 (6B1E Chain A) protein receptor binding pocket, the rGyr fluctuations of flazin, quercetin 3,4′-dimethyl ether, and 13-azaprostanoic acid remained almost constant, with rGyr values ranging from 3.72 to 3.90 Å, 3.84–3.96 Å and 4.80–5.60 Å, respectively. It was shown that the ligand was almost steady in 100 ns simulation time. According to the results of introHB, no intramolecular HB was detected when the DPP-4 (6B1E Chain A) protein was combined with flazin and 13-azaprostanoic acid. However, multiple intramolecular HB was found when combined with quercetin 3,4′-dimethyl ether. The MolSA values of flazin, quercetin 3,4′-dimethyl ether, and 13-azaprostanoic acid are 277–285 $Å^2$, 285–295 $Å^2$, 360–380 $Å^2$, respectively, and the PSA values are 160–180 $Å^2$, 184–208 $Å^2$, and 90–110 $Å^2$, respectively. In addition, the SASA values of these compounds are in the range of 80–240 $Å^2$, 80–320 $Å^2$, and 120–300 $Å^2$, respectively.

4. Conclusion

In this study, various polyherbal combinations of *S. grosvenorii (SG)*, *D. longan (DL)* and *O. stamineus (OS)* all showed anti-diabetic potential, and compared with single *S. grosvenorii* and *D. longan* extracts, different combinations all showed better anti-diabetic properties *in vitro*, which was further verified by computer analysis. In short, due to the hypoglycemic properties shown by the multi-extract combination, it could be further developed as a potential therapy for type 2 diabetes. Since this study is the first to combine *S. grosvenorii (SG)*, *D. longan (DL)* and *O. stamineus (OS)* and explore their combined anti-diabetic effects, more detailed practical and clinical trials may be needed to confirm their anti-hyperglycemic efficacy. Based on the results of this study, this multi-extract combinations can be further considered as a viable adjunctive formulation for diabetes prevention and treatment. At the same time, in addition to directly targeting diabetes, these combinations may also have other useful physiological activities, such as anti-lipids. Therefore, the multi-extract combination has a larger and broader metabolic pathway that we need to further explore.

CRediT authorship contribution statement

Jing Zhao: Data curation, Methodology, Formal analysis, Writing – original draft. **Douglas Law:** Funding acquisition, Writing – review & editing, Supervision. **Song Zhu:** Data curation. **Thiam-Tsui Tee:** Methodology. **Cheah Yew Hoong:** Funding acquisition, Writing – review & editing, Supervision. **Ahmed Najm:** Funding acquisition, Project administration, Supervision, Resources, Writing – review & editing. **Shazrul Fazry:** Funding acquisition, Project administration, Supervision, Resources, Writing – review & editing.

Declaration of competing interest

The authors declare that they have no known competing financial interests or personal relationships that could have appeared to influence the work reported in this paper.

Acknowledgments

This work was supported by Department of Food Sciences, Faculty Science and Technology, Universiti Kebangsaan Malaysia (Funding No.: ST-2019-013, UKM-TR-018, and ST-2021-010) and supported by Inti International University (INTI-FHLS-01-26-2023 and INTI-FHLS-01-03-2022).

Appendix A. Supplementary material

Supplementary data to this article can be found online at https://doi.org/10.1016/j.arabjc.2024.105733.

References

Ansari, P., Akther, S., Hannan, J.M.A., Seidel, V., Nujat, N.J., Abdel-Wahab, Y.H., 2022. Pharmacologically active phytomolecules isolated from traditional antidiabetic plants and their therapeutic role for the management of diabetes mellitus. Molecules 27 (13), 4278. https://doi.org/10.3390/molecules27134278.

Baby, K., Maity, S., Mehta, C.H., Nayak, U.Y., Shenoy, G.G., Pai, K.S.R., Harikumar, K.B., Nayak, Y., 2023. Computational drug repurposing of Akt-1 allosteric inhibitors for non-small cell lung cancer. Sci. Rep. 13 (1), 7947. https://doi.org/10.1038/s41598-023-35122-7.

Basnet, S., Ghimire, M.P., Lamichhane, T.R., Adhikari, R., Adhikari, A., 2023. Identification of potential human pancreatic α-amylase inhibitors from natural products by molecular docking, MM/GBSA calculations, MD simulations, and ADMET analysis. PLoS One 18 (3), e0275765.

Bassalat, N., Kadan, S., Melamed, S., Yaron, T., Tietel, Z., Karam, D., Kmail, A., Masalha, M., Zaid, H., 2023. *In vivo* and *in vitro* antidiabetic efficacy of aqueous and methanolic extracts of *Orthosiphon Stamineus* benth. Pharmaceutics 15 (3), 945. https://doi.org/10.3390/pharmaceutics15030945.

Bhakhar, K.A., Gajjar, N.D., Bodiwala, K.B., Sureja, D.K., Dhameliya, T.M., 2021. Identification of anti-mycobacterial agents against mmpL3: virtual screening,

ADMET analysis and MD simulations. J. Mol. Struct. 1244, 130941 https://doi.org/10.1016/j.molstruc.2021.130941.
Bibi, N., Shah, M.H., Khan, N., Al-Hashimi, A., Elshikh, M.S., Iqbal, A., Ahmad, S., Abbasi, A.M., 2022. Variations in total phenolic, total flavonoid contents, and free radicals' scavenging potential of onion varieties planted under diverse environmental conditions. Plants 11 (7), 950. https://doi.org/10.3390/plants11070950.
Chaipoot, S., Punfa, W., Ounjaijean, S., Phongphisutthinant, R., Kulprachakarn, K., Parklak, W., Phaworn, L., Rotphet, P., Boonyapranai, K., 2022. Antioxidant, anti-diabetic, anti-obesity, and antihypertensive properties of protein hydrolysate and peptide fractions from black sesame cake. Molecules 28 (1), 211. https://doi.org/10.3390/molecules28010211.
Chen, J., Xie, Q., Miao, W., Fan, J., Zhou, X., Li, M., 2022. CircPDHX promotes prostate cancer cell progression in vitro and tumor growth in vivo via miR-497-5p/ACSL1 axis. Biochem. Biophys. Res. Commun. 620, 35–41. https://doi.org/10.1016/j.bbrc.2022.06.012.
Dappula, S.S., Kandrakonda, Y.R., Shaik, J.B., Mothukuru, S.L., Lebaka, V.R., Mannarapu, M., Amooru, G.D., 2023. Biosynthesis of zinc oxide nanoparticles using aqueous extract of Andrographis alata: characterization, optimization and assessment of their antibacterial, antioxidant, antidiabetic and anti-Alzheimer's properties. J. Mol. Struct. 1273, 134264 https://doi.org/10.1016/j.molstruc.2022.134264.
Entezari, M., Hashemi, D., Taheriazam, A., Zabolian, A., Mohammadi, S., Fakhri, F., Hashemi, M., Hushmandi, K., Ashrafizadeh, M., Zarrabi, A., Ertas, Y.N., 2022. AMPK signaling in diabetes mellitus, insulin resistance and diabetic complications: a pre-clinical and clinical investigation. Biomed. Pharmacother. 146, 112563 https://doi.org/10.1016/j.biopha.2021.112563.
Gajjar, N.D., Dhameliya, T.M., Shah, G.B., 2021. In search of RdRp and Mpro inhibitors against SARS CoV-2: molecular docking, molecular dynamic simulations and ADMET analysis. J. Mol. Struct. 1239, 130488 https://doi.org/10.1016/j.molstruc.2021.130488.
Gong, P., Guo, Y., Chen, X., Cui, D., Wang, M., Yang, W., Chen, F., 2022. Structural characteristics, antioxidant and hypoglycemic activities of polysaccharide from *siraitia grosvenorii*. Molecules 27 (13), 4192. https://doi.org/10.3390/molecules27134192.
Gulcin, İ., Alwasel, S.H., 2023. DPPH radical scavenging assay. Processes 11 (8), 2248. https://doi.org/10.3390/pr11082248.
Hajji, H., Alaqarbeh, M., Lakhlifi, T., Ajana, M.A., Alsakhen, N., Bouachrine, M., 2022. Computational approach investigation bioactive molecules from *Saussurea Costus* plant as SARS-CoV-2 main protease inhibitors using reverse docking, molecular dynamics simulation, and pharmacokinetic ADMET parameters. Comput. Biol. Med. 150, 106209 https://doi.org/10.1016/j.compbiomed.2022.106209.
Huneif, M.A., Alshehri, D.B., Alshaibari, K.S., Dammaj, M.Z., Mahnashi, M.H., Majid, S. U., Javed, M.A., Ahmad, S., Rashid, U., Sadiq, A., 2022. Design, synthesis and bioevaluation of new vanillin hybrid as multitarget inhibitor of α-glucosidase, α-amylase, PTP-1B and DPP4 for the treatment of type-II diabetes. Biomed. Pharmacother. 150, 113038 https://doi.org/10.1016/j.biopha.2022.113038.
Hussain, A., Hussain, A., Sabnam, N., Verma, C.K., Shrivastava, N., 2023. Insilico exploration of the potential inhibitory activity of DrugBank compounds against CDK7 kinase using structure-based virtual screening, molecular docking, and dynamics simulation approach. Arab. J. Chem. 16 (2), 104460 https://doi.org/10.1016/j.arabjc.2022.104460.
Liu, J., Liu, M., Chai, Z., Li, C., Wang, Y., Shen, M., Zhuang, G., Zhang, L., 2023. Projected rapid growth in diabetes disease burden and economic burden in China: a spatio-temporal study from 2020 to 2030. Lancet Regional Health-Western Pacific 33. https://doi.org/10.1016/j.lanwpc.2023.100700.
Liu, W., Luo, Z., Zhou, J., Sun, B., 2022. Gut microbiota and antidiabetic drugs: perspectives of personalized treatment in type 2 diabetes mellitus. Front. Cell. Infect. Microbiol. 12, 853771 https://doi.org/10.3389/fcimb.2022.853771.
Liu, H., Qi, X., Yu, K., Lu, A., Lin, K., Zhu, J., Zhang, M., Sun, Z., 2019. AMPK activation is involved in hypoglycemic and hypolipidemic activities of mogroside-rich extract from Siraitia grosvenorii (swingle) fruits on high-fat diet/streptozotocin-induced diabetic mice. Food Funct. 10 (1), 151–162. https://doi.org/10.1039/C8FO01486H.
Liu, L., Zheng, J., Zhou, M., Li, S., He, G., Wu, J., 2021. Peptide analogues of VPP and IPP with improved glucose uptake activity in L6 myotubes can be released from cereal proteins. J. Agric. Food Chem. 69 (9), 2875–2883. https://doi.org/10.1021/acs.jafc.1c00587.
Moens, C., Muller, C.J., Bouwens, L., 2022. In vitro comparison of various antioxidants and flavonoids from rooibos as beta cell protectants against lipotoxicity and oxidative stress-induced cell death. PLoS One 17 (5), e0268551.
Mohamed, W.A.S., Ismail, N.Z., Muhamad, M., Omar, E.A., Samad, N.A., Ooi, J.P., Mohamad, S., 2022. Q-TOF LC-MS compounds evaluation of propolis extract derived from Malaysian stingless bees, Tetrigona apicalis, and their bioactivities in breast cancer cell, MCF7. Saudi J. Biol. Sci. 29 (10), 103403 https://doi.org/10.1016/j.sjbs.2022.103403.
Nguyen, P.H., Tuan, H.N., Hoang, D.T., Vu, Q.T., Pham, M.Q., Tran, M.H. and To, D.C., 2019. Glucose uptake stimulatory and PTP1B inhibitory activities of pimarane diterpenes from *Orthosiphon stamineus* Benth. *Biomolecules*, 9(12), p.859. doi: 10.3390/biom9120859.
Perumal, N., Nallappan, M., Shohaimi, S., Kassim, N.K., Tee, T.T. and Cheah, Y.H., 2022. Synergistic antidiabetic activity of Taraxacum officinale (L.) Weber ex FH Wigg and Momordica charantia L. polyherbal combination. *Biomedicine & Pharmacotherapy*, 145, p.112401. doi:10.1016/j.biopha.2021.112401.
Rahman, M.M., Dhar, P.S., Anika, F., Ahmed, L., Islam, M.R., Sultana, N.A., Cavalu, S., Pop, O., Rauf, A., 2022. Exploring the plant-derived bioactive substances as antidiabetic agent: an extensive review. Biomed. Pharmacother. 152, 113217 https://doi.org/10.1016/j.biopha.2022.113217.
Rakariyatham, K., Zhou, D., Rakariyatham, N., Shahidi, F., 2020. Sapindaceae (Dimocarpus longan and Nephelium lappaceum) seed and peel by-products: potential sources for phenolic compounds and use as functional ingredients in food and health applications. J. Funct. Foods 67, 103846. https://doi.org/10.1016/j.jff.2020.103846.
Salahuddin, M.A.H., Ismail, A., Kassim, N.K., Hamid, M., Ali, M.S.M., 2020. Phenolic profiling and evaluation of in vitro antioxidant, α-glucosidase and α-amylase inhibitory activities of Lepisanthes fruticosa (Roxb) Leenh fruit extracts. Food Chem. 331, 127240 https://doi.org/10.1016/j.foodchem.2020.127240.
Shahid, M., Fazry, S., Azfaralariff, A., Najm, A.A.K., Law, D., Mackeen, M.M., 2023. Bioactive compound identification and in vitro evaluation of antidiabetic and cytotoxic potential of *Garcinia atroviridis* fruit extract. Food Biosci. 51, 102285 https://doi.org/10.1016/j.fbio.2022.102285.
Tomic, D., Shaw, J.E., Magliano, D.J., 2022. The burden and risks of emerging complications of diabetes mellitus. Nat. Rev. Endocrinol. 18 (9), 525–539. https://doi.org/10.1038/s41574-022-00690-7.
Wang, Q., Wang, J., Li, N., Liu, J., Zhou, J., Zhuang, P., Chen, H., 2022. A systematic review of *Orthosiphon stamineus* Benth. in the treatment of diabetes and its complications. Molecules 27 (2), 444. https://doi.org/10.1038/s41574-022-00690-7.
Yin, R., Xu, Y., Wang, X., Yang, L., Zhao, D., 2022. Role of dipeptidyl peptidase 4 inhibitors in antidiabetic treatment. Molecules 27 (10), 3055. https://doi.org/10.3390/molecules27103055.
Yusuf, A.P., Zhang, J.Y., Li, J.Q., Muhammad, A., Abubakar, M.B., 2022. Herbal medications and natural products for patients with covid-19 and diabetes mellitus: potentials and challenges. Phytomedicine plus 2 (3), 100280. https://doi.org/10.1016/j.phyplu.2022.100280.
Zhang, Y., Peng, Y., Zhao, L., Zhou, G., Li, X., 2021. Regulating the gut microbiota and SCFAs in the faeces of T2DM rats should be one of antidiabetic mechanisms of mogrosides in the fruits of *Siraitia grosvenorii*. J. Ethnopharmacol. 274, 114033 https://doi.org/10.1016/j.jep.2021.114033.